Mechanics-Guided Optimization of Dimensional Fidelity in Continuous Basalt Fiber-Reinforced PLA

Mohammad Nowfel Mahiuddin [1], Prasenjit Chatterjee [2]

[1] Department of Mechanical Engineering, Lincoln University College, 47301 Petaling Jaya, Malaysia;

[2] Department of Mechanical Engineering, MCKV Institute of Engineering, Howrah, West Bengal - 711204, India.

Email ID: pdf.nowfelmahiuddin@lincoln.edu.my[1]

chatterjee.drprasenjit@gmail.com[2]

Abstract: Continuous-fiber reinforcement is one of the most practical ways to turn material-extrusion 3D printing into a process suitable for structural applications. Basalt fiber is particularly interesting here because it offers stiffness comparable to glass fiber and comes from a single natural mineral source, making it a potentially more sustainable option [1]. However, there is a key challenge. When a stiff fiber is embedded into a semi-molten thermoplastic during printing, the print head has to guide it through curves and corners. This often leads to small deviations from the intended path, especially at sharp turns. These errors can shift fiber placement, change wall thickness, and create stress concentrations, issues that are critical in anisotropic composite materials [2].

In this work, we propose a mechanics-based framework to improve dimensional accuracy in continuous basalt fiber-reinforced PLA (CBF-PLA). The approach introduces a printable-curvature criterion that connects fiber tension, nozzle design, and interfacial behavior to the maximum achievable curvature. It also includes a structured experimental plan to separately evaluate global warping and local geometric deviations. By treating toolpath smoothing and corner compensation as key design variables, the framework offers a clear, mechanism-driven way to achieve more reliable and accurate printed structures.

Keywords: Continuous basalt fiber; material extrusion additive manufacturing; fused filament fabrication; dimensional fidelity; trajectory error; sustainable composites.

Introduction

Material extrusion additive manufacturing (ME-AM), including fused filament fabrication (FFF), can create thin-walled and multi-cell topologies with minimal tooling, which is why it is often proposed for lightweight structural concepts. The problem is that fidelity is not guaranteed. Thermal gradients during deposition generate residual stresses and, even in neat polymers, these stresses can drive shrinkage and warpage with strong sensitivity to process settings such as speed, temperature, and layer height [3].

Continuous-fiber ME-AM changes the failure physics. In in-nozzle impregnation architectures, the polymer filament melts inside the print head and consolidates a continuous fiber bundle in the heated region just before extrusion [4]. Once the bead exits the nozzle, the system is no longer just placing a viscous polymer. It is steering a reinforcement tow that resists bending and is often tensioned by friction and kinematic transients. Process-induced defects in continuous-fiber thermoplastic printing, including fiber waviness, folding, and trajectory error, are now treated as central barriers to performance and robustness [5].

Basalt fiber is mechanically "stiff enough" that the steering problem matters. Representative manufacturer-reported basalt fiber modulus values around 90 GPa are close to E-glass and far below high-modulus carbon, yet still high enough that fiber tension and curvature enforcement can dominate corner fidelity [6]. Continuous basalt-fiber thermoplastic composites also show strong anisotropy; longitudinal properties can greatly exceed transverse and shear responses [2]. This anisotropy makes geometry control more important, not less, because small geometric deviations can shift load paths and failure initiation sites.

This manuscript reframes dimensional fidelity for CBF-PLA as a coupled mechanics and heat-transfer problem that can be treated systematically. We refine the original conference draft into a submission-ready structure by (a) stating four testable hypotheses (H1–H4) with scan-visible signatures, (b) introducing a printable-curvature criterion that converts corner-cutting into a measurable limit state, and (c) specifying a metrology and DOE pathway intended to produce transferable, mechanism-linked process windows.

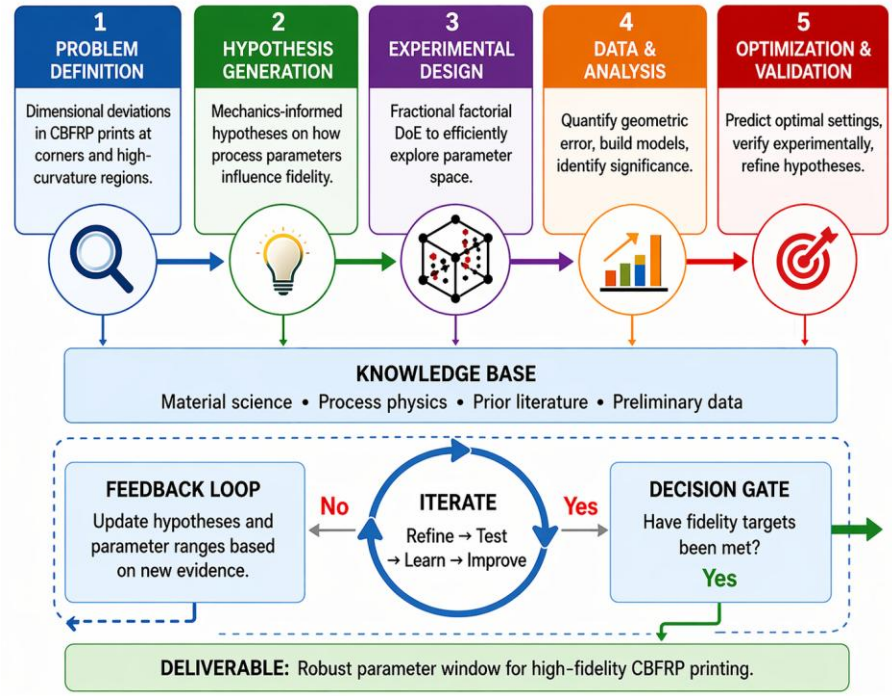

Figure 1. Mechanics-guided workflow for improving dimensional fidelity in continuous basalt fiber-reinforced PLA (CBF-PLA), linking hypotheses and mechanics to DOE, metrology, and a validated process window.

Framework and governing mechanics

A practical CBF-PLA process context is helpful. Continuous-fiber printers span multiple architectures, but the present framework assumes an in-nozzle impregnation head in which fiber consolidation occurs in the heated region of the nozzle [4]. In this class of systems, nozzle diameter and tow diameter are not merely "printer settings." They influence bead geometry, impregnation stability, and the magnitude of curved-path trajectory errors; accordingly, they must be treated as first-order variables in any fidelity study [7].

Printable-curvature criterion. Curvature-related trajectory deviation is repeatedly reported as a dominant failure mode in continuous-fiber printing. Liu and colleagues formalize this behavior through a maximum printable curvature and use it as the basis for compensation [7]. We adopt the same physical intuition, but restate it as a corner-followability condition for dimensional fidelity.

A tow under axial tension T forced to follow a planar curvature $\kappa = 1/R$ requires a distributed normal reaction on the order of $T\kappa$ to remain on path. The semi-molten bead can only supply a limited reaction, which we approximate as an effective interfacial shear capacity τ_{int} acting over a characteristic bead width b. This defines a curvature limit:

$$\kappa_{\max} \approx \frac{\tau_{\text{int}}\, b}{T} \quad \ldots\ldots\ldots\ldots\ldots\ldots\ldots\ldots\ldots\ldots\ldots\ldots (1)$$

When $\kappa_{\text{required}} > \kappa_{\max}$, the fiber cannot be held to the commanded toolpath and relaxes to a lower curvature, producing corner-cutting, tow waviness, and (in severe cases) folding and breakage [7]. Eq. (1) is valuable mainly because it isolates the dependencies that matter for optimization: $\kappa_{\max}$ decreases if tension rises (speed and acceleration transients, frictional drag, tow routing) and increases if interfacial shear capacity rises (wetting, compaction, thermal history, and the time available for bead stiffening) [5].

A local geometric metric follows. Define δ as an inset distance between the commanded corner and realized fiber path, measured along the 45° bisector for a 90° turn. If the realized tangent radius is R_{act} and the commanded toolpath fillet radius is R_{cmd}, a convenient approximation is:

$$\delta \approx \left(\sqrt{2} - 1\right) \max(0,\, R_{\text{act}} - R_{\text{cmd}}), \quad R_{\text{act}} = 1/\kappa_{\max} \quad \ldots\ldots\ldots\ldots\ldots\ldots\ldots\ldots (2)$$

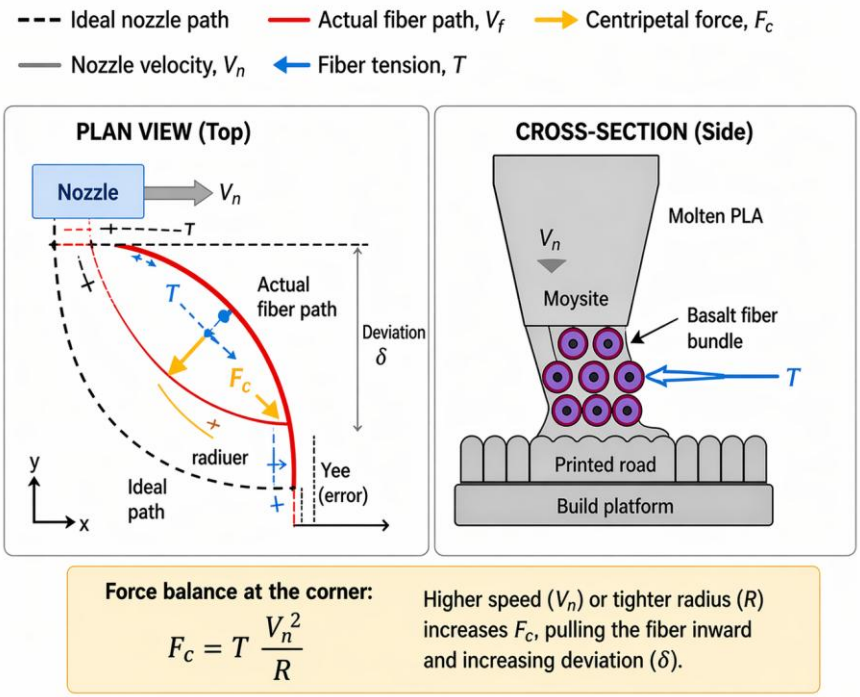

Figure 2. Corner-cutting in continuous-fiber ME-AM and the role of path smoothing.

Figure 2 illustrates the qualitative geometry and emphasizes that reducing $\kappa_{\mathrm{required}}$ at the toolpath level is often the most direct way to suppress corner deviation.

Four hypotheses as testable mechanisms. The original manuscript proposed four hypotheses; here they are rewritten as falsifiable statements with explicit signatures and levers.

H1 (internal bracing and residual stress): Continuous basalt fibers suppress axial thermal contraction along the tow direction, while the PLA matrix still contracts during cooling. The mismatch generates residual stresses that manifest as global bowing or warpage, especially in thin walls. Thermomechanical modeling and optimization studies of polymer FDM parts support the central relevance of thermal history in distortion [8][9].

H2 (speed–tension interaction): Higher print speed and aggressive acceleration increase tow tension and reduce time for local bead stiffening at corners, lowering $\kappa_{\max}$ and increasing δ. Trajectory error in continuous-fiber printing shows strong curvature sensitivity and explicitly links nozzle and tow diameters to curved-track errors [7].

H3 (compaction-controlled interlayer bonding): An intermediate layer height and extrusion multiplier maximize fidelity by ensuring consistent tow embedding and interlayer contact without bead bulging or over-extrusion. Dimensional-accuracy literature for FDM emphasizes layer height and thermal settings; continuous fiber adds the requirement that the tow be placed at a repeatable depth with sufficient interfacial contact [3].

H4 (toolpath curvature management): Toolpath smoothing, fillets, and explicit corner compensation reduce $\kappa_{\mathrm{required}}$ and move printing from $\kappa_{\mathrm{required}} > \kappa_{\max}$ to $\kappa_{\mathrm{required}} \leq \kappa_{\max}$. Corner-optimization studies in continuous-fiber FFF report large improvements in angle fit and printing reliability when toolpaths are compensated at corners [10].

Experimental program and metrology

A high-quality dimensional-fidelity study should not collapse “error” into a single number. That practice hides mechanisms and usually produces recipes that do not transfer. The proposed program separates error modes at the measurement level and uses staged DOE to connect each mode to an actionable parameter set.

Printing system description. As a baseline, the in-nozzle impregnation architecture demonstrated by Matsuzaki and colleagues provides a reproducible reference for continuous-fiber ME-AM [4]. In a CBF-PLA implementation, the print head must accommodate tow diameter, limit tow folding in curved motion, and maintain stable bead geometry. Because trajectory-error models depend on nozzle diameter and tow diameter, these geometric details should be reported explicitly and controlled during optimization [7].

Response variables. We define three primary outcome measures, all assessed after cooldown:

Warpage W: out-of-plane displacement of nominally planar features, reported as maximum and RMS deviation.

Corner deviation δ: inset distance at specified corners, extracted from the tow centerline in a scan and measured directly or via Eq. (2).

Thickness drift Δt: deviation of wall thickness (or bead height) from nominal along straight segments and near corners.

A structured-light 3D scanner provides full-field geometry for W and enables repeated extraction of δ. A coordinate measuring machine can provide reference datums when needed. This aligns with additive manufacturing capability assessment practice; ISO [11] /ASTM 52902 defines benchmarking test artifacts and the quantitative measurements used to evaluate geometric capability (ISO, 2019) [12]. Microstructural checks (cross-sections for tow depth and void fraction) should be used to connect geometry to consolidation quality and to the τ_{int} term in Eq. (1).

Staged DOE and toolpath interventions. A full factorial across kinematic, thermal, and toolpath variables becomes unmanageably large. Instead, a staged approach is both practical and consistent with published warpage-optimization strategies in polymer printing and with defect-focused reviews of continuous-fiber thermoplastic printing [8].

Stage A (screening under fixed toolpath): use a Taguchi-style screening design or definitive screening design to rank effects across print speed v, a kinematic transient proxy (acceleration a or jerk limits), layer height h, extrusion multiplier E, nozzle temperature T_n, bed temperature T_b, and cooling settings [8].

Stage B (curvature study at fixed "best" process settings): print a curvature benchmark set spanning sharp corners ($R_{\mathrm{cmd}} = 0$) and fillets ($R_{\mathrm{cmd}} = 0.5{,}1{,}2{,}3$ mm). In parallel, apply a corner compensation routine in G-code. This is motivated directly by continuous-fiber corner-optimization work showing large improvements in corner fit and reliability [10].

Stage C (refinement and interaction mapping): fit a response surface in the reduced parameter subspace for W, δ, and Δt. Where the surface is strongly nonlinear, adopt a surrogate-assisted approach; DOE-guided neural-network models have been used to predict and optimize dimensional accuracy in FDM while reducing experimental burden [11].

The deliverable is a process window explicitly connected to H1–H4 and to the limit state in Eq. (1), rather than a one-off tuning recipe.

Table 1. Representative reinforcement-fiber properties (manufacturer datasheet value reported by Kessler et al.) [6]

Property (fiber-only)	Basalt fiber	E-glass fiber	Carbon fiber (T700 class)
Fiber diameter (µm)	13–20	17	7
Density (g/cm³)	2.6	2.45	1.8
Tensile strength (MPa)	2850	2450	4900
Tensile modulus (GPa)	90	80	230

Table 2. Hypotheses, expected scan signatures, and first-response levers for dimensional fidelity in CBF-PLA

Hypothesis	Dominant mechanism	What you expect to see	Primary levers	Secondary check
H1	thermal mismatch + internal bracing	global warpage W, twist, edge lift	T_b, enclosure, cooling strategy, raster strategy	correlate W with cooldown history
H2	speed-driven tension + reduced $\kappa_{\max}$	increased δ, tow waviness, fold initiation	v, a/jerk, corner speed limits	repeatability and failure frequency at corners
H3	compaction + interlayer shear	Δt drift, bead bulging, local delamination	h, E, T_n	tow depth and void fraction from cross-sections
H4	toolpath curvature management	δ decreases with R_{cmd}	fillets, compensation, smoothing	verify $\kappa_{\mathrm{required}} \leq \kappa_{\max}$ trends

Table 3. Illustrative starting ranges for staged fidelity optimization (to be adapted to printer limits and tow size)

Parameter	Symbol	Screening range
Print speed (mm/min)	v	100–600
Acceleration (mm/s²) or jerk proxy	a	printer-specific
Layer height (mm)	h	0.20–0.30
Extrusion multiplier	E	0.90–1.10
Nozzle temperature (°C)	T_n	200–240
Bed temperature (°C)	T_b	40–70
Fillet radius (mm)	R_{cmd}	0–3

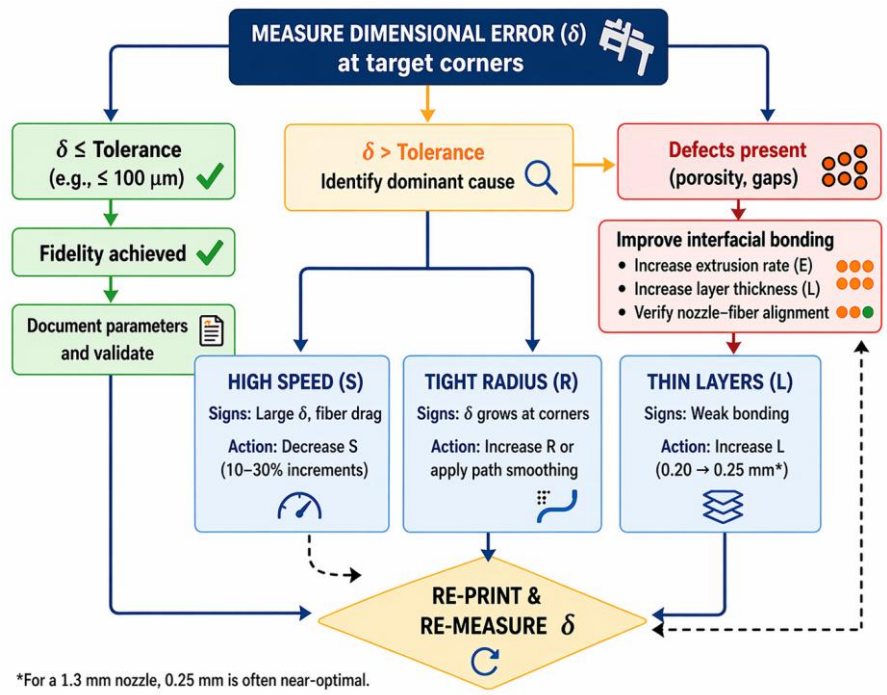

Figure 3. Diagnostic decision tree that maps observed non-compliance (warpage, corner deviation, thickness drift, or impregnation-related defects) to the underlying hypotheses and first-response parameter levers.

Model-informed expected trends and discussion

Eq. (1) imposes structure on experiments. It predicts that corner deviation escalates when the combination of tension T and required curvature κ_{required} overwhelms interfacial capacity $\tau_{\text{int}}b$. That is consistent with curved-track trajectory-error modeling, which motivates compensation based on maximum printable curvature [7].

Three trends should be visible in scan data.

First, speed effects should be geometry dependent. On straight tracks, increasing v may have weak geometric impact if deposition remains stable. At corners, the same speed increase can produce larger tension transients and less time for bead stiffening, increasing δ [7].

Second, toolpath smoothing should behave like a first-class control knob. Raising R_{cmd} lowers κ_{required}. Corner-optimization work in continuous-fiber FFF confirms that explicit corner compensation can substantially improve corner fit and printing reliability, which is exactly what H4 predicts [10].

Third, thermal settings must remain in the design even if the question is “mostly kinematic.” Residual stress and warpage in printed PLA correlate strongly with thermal history, and digital-twin-type approaches have been validated for reducing residual stress in printed PLA thin walls [9]. In CBF-PLA, the tow acts as an internal constraint, so thermal settings that reduce warpage in neat PLA can shift the balance among W, δ, and Δt. That interplay is why H1 is not treated as a secondary effect.

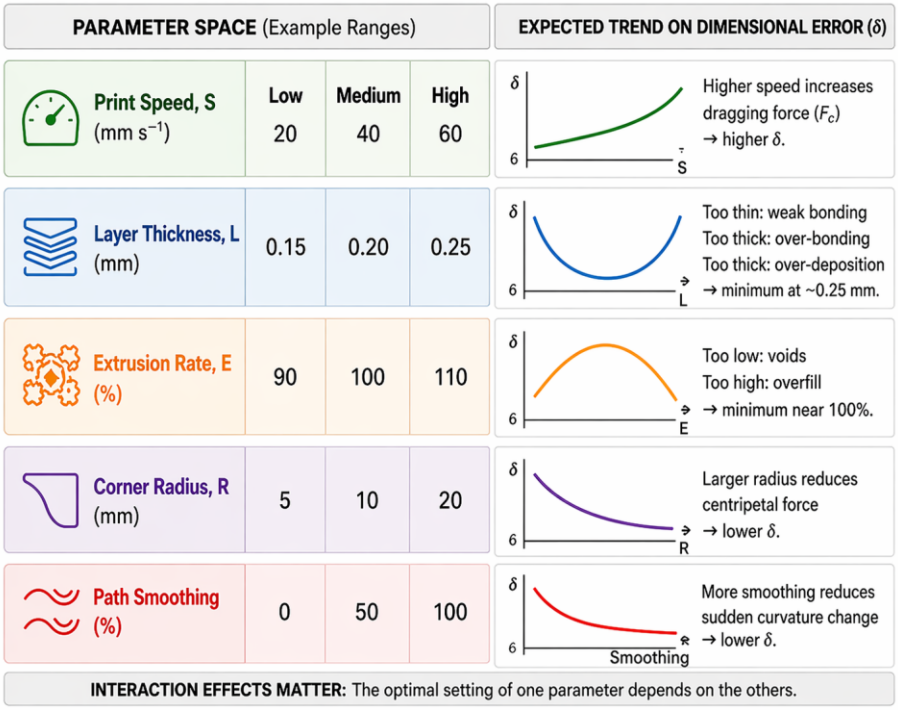

Figure 4. Illustrative scaling prediction based on Eq. (2). Increasing R_{cmd} suppresses corner deviation δ and reduces sensitivity to print speed once the commanded curvature is well below the printable limit.

Figure 4 provides an illustrative scaling prediction based on Eq. (2): if the effective interfacial capacity decreases with increasing v (a proxy for reduced time for bead stiffening at corners), then δ increases with v, while increasing R_{cmd} collapses δ and can reduce sensitivity to v once commanded curvature is well below the printable limit.

Limitations and validation requirements. A full research manuscript ultimately needs data. For CBF-PLA, convincing validation should include (i) a quantitative scan dataset across the staged DOE; (ii) evidence that the curvature criterion anticipates the onset of corner failure or excessive δ; and (iii) microstructural evidence linking process settings to tow placement and void fraction in a way consistent with changes in τ_{int}. The payoff is that the framework makes those validation steps more efficient by telling you what to measure and why [5].

Finally, the framework is compatible with data-efficient optimization. DOE-guided surrogate modeling has been used to predict and optimize dimensional accuracy in FDM [11] and continuous-fiber composite printing has begun to incorporate machine-learning-based monitoring and closed-loop control [13]. A physics-guided surrogate in which $\kappa_{\max}$ acts as a soft constraint is a natural next step once a baseline dataset exists for your printer-material system.

Conclusion and outlook

Dimensional fidelity in continuous basalt fiber-reinforced PLA is a coupled mechanics and thermal problem, and it becomes sharpest at corners where fiber steering is tension limited. This manuscript

refines a hypothesis-driven framework by adding a printable-curvature criterion, defining distinct metrology targets (W, δ, Δt), and proposing a staged DOE that includes both kinematic and thermal levers.

If there is one practical takeaway, it is that curvature should be treated as a limit state. When $\kappa_{\mathrm{required}}$ approaches $\kappa_{\max}$, corner deviation is an expected consequence of tow tension overpowering a weakly consolidated bead. Two levers then dominate. You can lower $\kappa_{\mathrm{required}}$ through toolpath design (fillets, corner compensation, corner speed limits). You can raise $\kappa_{\max}$ by changing consolidation physics (temperature, cooling, compaction, bead width, and tow tension control). The framework's job is to make those levers explicit, measurable, and eventually predictive.

References

1. X. Zhang, V. Fiore, T. Scalici, G. Di Bella, and A. Valenza, "A review on basalt fibre and its composites," *Composites Part B: Engineering*, vol. 74, pp. 74–94, 2015, doi: 10.1016/j.compositesb.2014.12.034.
2. M. X. Zanelli, G. Ronconi, N. Pritoni, A. D'Iorio, M. Bertoldo, V. Mazzanti, and F. Mollica, "3D printing of continuous basalt fiber-reinforced composites: Characterization of the in-plane mechanical properties and anisotropy evaluation," *Polymers*, vol. 16, no. 23, p. 3377, 2024, doi: 10.3390/polym16233377.
3. B. Zharylkassyn, A. Perveen, and D. Talamona, "Effect of process parameters and materials on the dimensional accuracy of FDM parts," Materials Today: Proceedings, 2021, doi: 10.1016/j.matpr.2020.11.332.
4. R. Matsuzaki, M. Ueda, M. Namiki, T. K. Jeong, H. Asahara, K. Horiguchi, T. Nakamura, A. Todoroki, and Y. Hirano, "Three-dimensional printing of continuous-fiber composites by in-nozzle impregnation," Scientific Reports, vol. 6, p. 23058, 2016, doi: 10.1038/srep23058.
5. W. Zhu et al., "Three-dimensional printing of high-performance continuous fiber-reinforced thermoplastic composites: Causes and elimination of process-induced defects," Composites Part B: Engineering, vol. 292, p. 112080, 2025, doi: 10.1016/j.compositesb.2024.112080.
6. E. Kessler, R. Gadow, and J. Straub, "Basalt, glass and carbon fibers and their fiber reinforced polymer composites under thermal and mechanical load," AIMS Materials Science, vol. 3, no. 4, pp. 1561–1576, 2016, doi: 10.3934/matersci.2016.4.1561.
7. M. Liu, S. Qu, S. Li, X. Yan, W. Li, and Y. Wang, "Modeling and compensation methods for trajectory errors in continuous fiber-reinforced thermoplastic composites using 3D printing," Polymers, vol. 17, no. 13, p. 1865, 2025, doi: 10.3390/polym17131865.
8. D. Syrlybayev, B. Zharylkassyn, A. Seisekulova, A. Perveen, and D. Talamona, "Optimization of the warpage of fused deposition modeling parts using finite element method," Polymers, vol. 13, no. 21, p. 3849, 2021, doi: 10.3390/polym13213849.
9. R. Viano, L. Demont, P. Margerit, R. Mesnil, J.-F. Caron, and D. Weisz-Patrault, "Residual stress control in large-format additive manufacturing of polylactic acid via a digital twin and in-

operando imaging," Materials & Design, vol. 260, p. 114870, 2025, doi: 10.1016/j.matdes.2025.114870.

10. J. Liu, Y. Kang, C. Ma, and Y. Wang, "Research on a fiber corner compensation algorithm in a 3D printing layer of continuous fiber-reinforced composite materials," Applied Sciences, vol. 12, no. 13, p. 6687, 2022, doi: 10.3390/app12136687.
11. O. A. Mohamed, S. H. Masood, and J. L. Bhowmik, "Modeling, analysis, and optimization of dimensional accuracy of FDM-fabricated parts using definitive screening design and deep learning feedforward artificial neural network," Advanced Manufacturing, vol. 9, pp. 115–129, 2021, doi: 10.1007/s40436-020-00336-9.
12. ISO. (2023). ISO/ASTM 52902:2023 Additive manufacturing: Test artifacts: Geometric capability assessment of additive manufacturing systems. International Organization for Standardization. ISO/ASTM 52902:2023 - Additive manufacturing — Test artefacts — Geometric capability assessment of additive manufacturing systems
13. X. Chi, J. Xue, L. Jia, J. Yao, H. Miao, L. Wu, T. Liu, X. Tian, and D. Li, "Machine learning-based online monitoring and closed-loop controlling for 3D printing of continuous fiber-reinforced composites," Additive Manufacturing Frontiers, vol. 4, no. 2, p. 200196, 2025, doi: 10.1016/j.amf.2025.200196.